

## Accurate modeling of electron-hole binding in CuCl. I. Exciton states

Selvakumar V. Nair<sup>1</sup>, Junko Usukura<sup>2,3</sup>, and Eiji Tokunaga<sup>3</sup>

<sup>1</sup>Centre for Advanced Nanotechnology, University of Toronto, 170 College Street, Toronto, Ontario M5S 3E3, Canada

<sup>2</sup>Institute for Solid State Physics, University of Tokyo, 5-1-5 Kashiwanoha, Kashiwa, Chiba 277-8581, Japan

<sup>3</sup>Department of Physics, Tokyo University of Science, 1-3 Kagurazaka, Shinjuku-ku, Tokyo 162-8601, Japan



(Received 29 December 2019; revised 5 June 2020; accepted 15 July 2020; published 5 August 2020)

We present an accurate variational approach for calculating the ground and excited exciton states in CuCl, and provide detailed comparison with measured polariton energies of excited exciton states. Computed exciton energies and oscillator strengths allow us to reproduce the polariton dispersion of up to four exciton states with unprecedented accuracy. A reinterpretation of the observed  $1s$ -exciton binding energy shows that the actual Coulomb energy in the exciton ground state is more than 50% larger than the observed binding energy, with important consequences for calculation of exciton complexes such as the biexciton.

DOI: [10.1103/PhysRevB.102.075202](https://doi.org/10.1103/PhysRevB.102.075202)

### I. INTRODUCTION

Starting with the seminal work of Haken [1], it is well known that the strong longitudinal-optical (LO)-phonon coupling with charge carriers affects the electron and hole states and their complexes in polar semiconductors. In particular, in CuCl, the free-electron-hole pair has a polaron binding energy of more than 100 meV which is comparable to the exciton binding energy of about 200 meV [2]. Furthermore, CuCl is one of the few materials (along with Cu<sub>2</sub>O) in which the Rydberg series of excitons with  $n$  up to 4 have been observed [2–5]. It is a common practice [6] to describe these states using an effective dielectric constant between  $\epsilon_0$  and  $\epsilon_\infty$  and interpret the observed exciton binding energy as an effective Rydberg, where  $\epsilon_0$  and  $\epsilon_\infty$  are the static and optical dielectric constants, respectively. We show that this is a naive interpretation and leads to an erroneous description of the exciton state and its complexes. In particular, interpreting the exciton binding energy as the Rydberg leads to a large underestimation of the Coulomb energy in the exciton. This is traced to be the main reason why even the best variational calculation of binding energy of a biexciton in CuCl [7] gives a result that is only 70% of the experimental value, as discussed in the following paper [8]. Furthermore, the observed energies and oscillator strength of the exciton strongly deviate [2,6] respectively from the  $1/n^2$  and  $1/n^3$  dependence [9] on the principal quantum number ( $n$ ) expected for hydrogenic states. Owing to the small size of the exciton in CuCl, such discrepancies have been often attributed to unknown “central-cell corrections,” viz., deviations from the continuum picture used in the classic description of a Wannier exciton. We show that almost all of the deviation from the hydrogenic series energies and oscillator strengths can be accounted for by proper consideration of polaronic effects.

This is our central argument: While the free electron and hole in CuCl are strongly dressed by phonons, the Coulomb binding brings the electron-hole pair close together, forming an exciton state that is smaller than the individual polarons. Thus the electron-hole pair undresses during exciton

formation, and almost all of the energy in the exciton is Coulombic which greatly exceeds the observed binding energy by the polaron energies of the free particles. This is illustrated schematically in Fig. 1. In the higher excited states of the exciton, as the extension of the electron-hole pair increases, this undressing is only partial, and finally tends towards fully dressed free electron-hole pairs as the principal quantum number ( $n$ ) or the angular momentum ( $L$ ) increases.

Inclusion of polaron coupling into the electron-hole Hamiltonian has been discussed by many authors [1,10–14] and a Fröhlich polaron [15] picture is generally accepted as valid. For the free electrons and holes in CuCl, the Fröhlich-coupling parameter ( $\alpha$ ) is in the intermediate-coupling regime so that a variational treatment based on the Lee-Low-Pines (LLP) transformation [16] is appropriate [1]. Haken extended the LLP transformation of single particles to the exciton-phonon system by representing the wave function as a product of the excitonic state and a phonon cloud described by a coherent state. Pollmann and Büttner found a suitable ansatz for the displacement function in the phonon coherent state and derived an effective local Hamiltonian for the exciton-phonon system [10]. This approach was extended by Matsuura and Büttner to the  $2s$  and  $3s$  excited states of an  $L = 0$  exciton [13,14]. A more general approach that avoids the variational ansatz for the phonon displacement was developed by Iadonisi, Bassani, and Strinati (IBS) [17]. However, their method is practical only for nodeless wave functions and has been applied to the lowest exciton states with  $L = 0$ –4. Furthermore, in all these calculations, the exciton wave function has been treated variationally using a hydrogenic form.

In this paper we present an accurate calculation of exciton states in CuCl including the phonon coupling using Haken’s LLP transformation. For the lowest energy state of the exciton, for each angular momentum, we can avoid any further approximations by numerically integrating the resulting equations for the phonon displacement functions and exciton wave function. We refer to this as the generalized Iadonisi-Bassani-Strinati (GIBS) method. This procedure provides a reference for

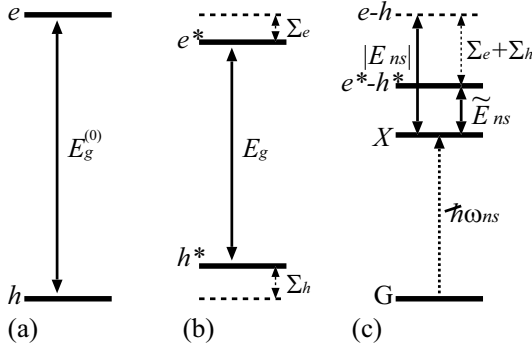


FIG. 1. Schematics of conduction band, valence band, and the exciton state. (a) The bare gap energy  $E_g^{(0)}$ . (b) The gap energy  $E_g$  measured experimentally, which is reduced from the bare gap by the polarization energy of a free electron-hole pair. (a) and (b) are represented in the single-particle picture. (c) The exciton state (X) in the multiparticle picture, which is excited optically by the excitation energy  $\hbar\omega_{ns}$ .  $|E_{ns}|$  corresponds to the difference between the bare gap and the excitation energy.  $e$  ( $h$ ) is a free electron (hole) not coupling to phonons and  $e^*$  ( $h^*$ ) is a free electron (hole) polaron.  $\tilde{E}_{ns}$  is the binding energy that could be experimentally measured.

further approximations necessary for relevant excited  $L = 0$  states ( $s$  states) which are readily observed in experiments.

An approach that applies to excited  $s$  states is the use of the Pollmann-Büttner ansatz for the phonon displacement. We find that this method gives results nearly identical to the more accurate numerical solution. Therefore, for the excited  $s$  states we use the Pollmann-Büttner ansatz for the phonon displacement but treat the exciton wave function numerically using a finite-difference discretization without assuming any functional forms.

In our formulation, orthogonalization constraints on the wave function are built into the calculation which have been neglected in the past [13,14]. The approximation using the partial orthogonality may reproduce measured binding energies fortuitously in some semiconductors in which excitons in all states are affected by phonons nearly to the same degree. In contrast, inaccuracy of the partial orthogonalization will be significant in semiconductors like CuCl, in which an exciton in the ground state undresses phonons while the undressing is only partial for excitons in excited states. This could partly explain the failure of past calculations to reproduce exciton energies in CuCl.

Optical properties of CuCl have been extensively studied experimentally. However, quantitative comparison with theory has so far met with limited success. The deviation of energies from  $1/n^2$  dependence mentioned above has only been qualitatively explained. Calculations that reproduce the relative energies of  $2s$  and  $3s$  excitons have failed to accurately predict the  $1s$  exciton energy [13,14]. In the first place, there are inconsistencies in the effective electron and hole masses used to calculate the energies of the excitons and the biexciton. Effective electron and hole masses of  $m_e \sim 0.4m_0$  and  $m_h \sim 4m_0$  were obtained by fitting exciton energy measurements and effective hydrogenic approximations, where  $m_0$  is the free electron mass. Meanwhile, the total mass of the exciton (center of mass) is accurately known to be  $2.3m_0$ , as obtained

directly from exciton dispersion measured by one photon absorption [18,19]. Not only does the sum of the electron and hole masses fail to agree with that of the center of mass, neglect of the state-dependent dressing of polarons in the exciton states leads to incorrect determination of parameters. Therefore, the effective electron and hole masses in CuCl should be reexamined. We determine effective electron and hole masses by fitting the calculated binding energies of  $n = 0-4$  states to experimental values. For the dielectric constants, both  $\epsilon_0$  and  $\epsilon_\infty$  are known from independent measurements and our approach does not require any phenomenological “effective” dielectric constant.

We also calculated the oscillator strengths of exciton states. In general, the phonon coupling acts to decrease oscillator strengths for excitons with increasing effect of phonons seen in higher excited states. As the energies and dispersion of exciton polariton states [20] are sensitive to the oscillator strengths, measured polariton dispersion [4,21,22] provide an excellent testing ground for our calculated results. A detailed comparison between predicted and observed polariton dispersion is presented.

## II. ELECTRON-HOLE INTERACTION INCLUDING FRÖHLICH COUPLING WITH LO PHONONS

The Hamiltonian describing the exciton coupled to phonons is written as

$$H = \frac{\hat{\mathbf{P}}^2}{2M} + \frac{\hat{\mathbf{p}}^2}{2\mu} - \frac{e^2}{\epsilon_\infty r} + \sum_{\mathbf{k}} \hbar\omega_0 a_{\mathbf{k}}^\dagger a_{\mathbf{k}} + \sum_{\mathbf{k}} [V_{\mathbf{k}} a_{\mathbf{k}} \rho_{\mathbf{k}}(\mathbf{r}) e^{i\mathbf{k}\cdot\mathbf{R}} + \text{H.c.}], \quad (1)$$

$$\rho_{\mathbf{k}}(\mathbf{r}) = e^{i\mathbf{s}_h \mathbf{k}\cdot\mathbf{r}} - e^{-i\mathbf{s}_e \mathbf{k}\cdot\mathbf{r}}, \quad (2)$$

where

$$V_{\mathbf{k}} = -\frac{i}{k} \sqrt{\frac{2\pi e^2 \hbar\omega_0}{V \epsilon^*}}, \quad (3)$$

$$\frac{1}{\epsilon^*} = \frac{1}{\epsilon_\infty} - \frac{1}{\epsilon_0}, \quad (4)$$

$\hat{\mathbf{P}}$  and  $\hat{\mathbf{p}}$  are conjugate momenta of the center of mass  $\mathbf{R}$  and the relative coordinate  $\mathbf{r}$ , respectively,  $\omega_0$  is the LO phonon frequency,  $M$  is the exciton mass,  $s_e = m_e/M$ ,  $s_h = m_h/M$ , and  $\mu$  is the reduced mass.

Following the LLP framework [16] we write a trial function for the  $nl$  exciton as

$$|\Phi_{nl}\rangle = T U_{nl} \varphi_{nl}(\mathbf{r}) |0\rangle. \quad (5)$$

The translational-motion operator and the coherent-state operator are given by

$$T = \exp \left[ i \left( \mathbf{Q} - \sum_{\mathbf{k}} a_{\mathbf{k}}^\dagger a_{\mathbf{k}} \mathbf{k} \right) \cdot \mathbf{R} \right], \quad (6)$$

and

$$U_{nl} \equiv U_{nl}(\mathbf{r}) = \exp \left\{ \sum_{\mathbf{k}} (F_{nl\mathbf{k}}^*(\mathbf{r}) a_{\mathbf{k}} - F_{nl\mathbf{k}}(\mathbf{r}) a_{\mathbf{k}}^\dagger) \right\}. \quad (7)$$

Here we set the total momentum  $\mathbf{Q}$  to zero to eliminate the center-of-mass motion from the wave function.

Minimization of the energy  $E = \langle \Phi_{nl} | H | \Phi_{nl} \rangle$  with respect to  $\varphi_{nl}$  gives the following equation for  $\varphi_{nl}$ :

$$\left[ \frac{\hbar^2}{2\mu} \nabla_r^2 - \frac{e^2}{\varepsilon_\infty r} + V_{\text{eff}}(\mathbf{r}) \right] \varphi_{nl}(\mathbf{r}) = E_{nl} \varphi_{nl}(\mathbf{r}), \quad (8)$$

where

$$V_{\text{eff}}(\mathbf{r}) = \frac{\hbar^2}{2\mu} \sum_k |\nabla_r F_{nlk}|^2 \sum_k \left( \hbar\omega_0 + \frac{\hbar^2 k^2}{2M} \right) |F_{nlk}|^2 - \sum_k (V_k \rho_k F_{nlk} + \text{H.c.}). \quad (9)$$

On the other hand, minimizing  $E$  with respect to  $F_{nl(k)}$  gives

$$-\frac{\hbar^2}{2\mu} \nabla^2 F_{nlk} - \frac{\hbar}{\mu} \frac{\nabla \varphi_{nl}(\mathbf{r})}{\varphi_{nl}(\mathbf{r})} \nabla F_{nlk} + \left( \frac{\hbar^2}{2\mu} + \frac{\hbar^2 k^2}{2M} \right) F_{nlk} = V_k \rho_k. \quad (10)$$

The coupled set of equations for  $\varphi_{nl}$  [Eq. (8)] and  $F_{nlk}$  [Eq. (10)] is to be solved self-consistently to determine the exciton states. This task is greatly simplified using a total angular momentum basis so that these equations may be reduced to a set of coupled ordinary differential equations [17]. However, unlike Ref. [17], we do not assume hydrogenic wave functions for  $\varphi_{nl}$ , and instead numerically integrate the differential equations.

As Eq. (10) involves  $\varphi_{nl}(\mathbf{r})$  in the denominator, the above approach is well defined only for exciton states with nodeless spatial wave function, viz., for the lowest state of each angular momentum ( $1s$ ,  $2p$ ,  $3d$ , ... states). As we are interested in excited zero angular momentum states ( $2s$ ,  $3s$ ,  $4s$ , ...), a modified approach is necessary. For this purpose, we take the Polmann-Büttner ansatz for the displacement amplitude [10],

$$F_{nlk}(\mathbf{r}) = \frac{V_k^*}{\hbar\omega_0} (f_{nlk}^{(e)} e^{-is_k \cdot \mathbf{r}} - f_{nlk}^{(h)} e^{is_k \cdot \mathbf{r}}), \quad (11)$$

and minimize the energy  $E = \langle \Phi_{nl} | H | \Phi_{nl} \rangle$  with respect to  $f_{nlk}^{(e)}$  and  $f_{nlk}^{(h)}$ ,

$$f_{nlk}^{(e)} = \frac{1 + R_h^2 k^2 (1 - G_n) - |G_n|^2}{(1 + R_e^2 k^2)(1 + R_h^2 k^2) - |G_n|^2}, \quad (12)$$

$$f_{nlk}^{(h)} = \frac{1 + R_e^2 k^2 (1 - G_n^*) - |G_n|^2}{(1 + R_w^2 k^2)(1 + R_h^2 k^2) - |G_n|^2}, \quad (13)$$

where  $G_n = \int d\mathbf{r} |\varphi_{nl}(\mathbf{r})|^2 e^{i\mathbf{k} \cdot \mathbf{r}}$  and  $R_i = \sqrt{\frac{\hbar}{2m_i \omega_0}}$ .

So far the Polmann-Büttner approach has been applied for exciton-phonon systems in various semiconductors. In these calculations [11,12], hydrogenlike functions with variational parameters were taken as the excitonic orbital parts of the wave functions  $\varphi_{nl}(\mathbf{r})$ . In Refs. [13,14] the binding energies and other properties for  $s$ - and  $p$ -wave excitons up to  $n = 3$  were calculated. However, in these studies the orthogonality was not strictly imposed on exciton states; not total wave functions  $|\Phi_{nl}\rangle$  but excitonic orbital functions  $\varphi_{nl}(\mathbf{r})$  were

orthogonalized to each other. For proper orthogonality,

$$\langle \Phi_{nl} | \Phi_{n'l} \rangle = \int d\mathbf{r} \varphi_{nl}^* \varphi_{n'l} \exp \left[ - \sum_k (F_{nlk} - F_{n'l k})^2 \right] = 0, \quad (14)$$

Eq. (8) is replaced with

$$\left[ \frac{\hbar^2}{2\mu} \nabla_r^2 - \frac{e^2}{\varepsilon_\infty r} + V_{\text{eff}}(\mathbf{r}) \right] \varphi_{nl}(\mathbf{r}) - \sum_{n' < n} \lambda_{n'} \exp \left[ - \sum_k (F_{nlk} - F_{n'l k})^2 / 2 \right] \varphi_{n'l}(\mathbf{r}) = E_{nl} \varphi_{nl}(\mathbf{r}), \quad (15)$$

and the left-hand side of Eq. (10) acquires an additional term of

$$\sum_{n' < n} \lambda_{n'} \exp \left[ - \sum_k (F_{nlk} - F_{n'l k})^2 / 2 \right] (F_{nlk} - F_{n'l k}) \frac{\varphi_{n'l}(\mathbf{r})}{\varphi_{nl}(\mathbf{r})}. \quad (16)$$

Here we make two improvements in the calculation process: One is that we numerically calculate  $\varphi_{ns}(r)$  by solving the differential equation (15) using a finite-difference approach. The other is that we impose the orthogonality of total wave functions. We apply this generalized Polmann-Büttner (GPB) method to calculate the  $s$ -wave excitons with  $n = 1-4$  in CuCl.

The transverse exciton mass has been estimated to be in the range  $M = 2.0m_0-3.0m_0$  from experiments [18,19,23,24]. We use  $M = 2.3m_0$  following the analysis of exciton dispersion obtained from two-photon Raman scattering [18]. The only unknown parameter is the electron-hole mass ratio, which is determined so that the binding energy for the  $2p$  state calculated by the GIBS method matches the measured values with all other parameters fixed at  $M = 2.3m_0$ ,  $\hbar\omega_0 = 25.6$  meV [25],  $\varepsilon_0 = 6.1$  [26], and  $\varepsilon_\infty = 3.7$  [27]. This procedure gives a value of  $\frac{m_e}{m_h} = 0.18$ . We list all the parameters used in the present calculation in the first row in Table I.

The exciton energies calculated by GPB and GIBS methods are listed in Table II and the corresponding wave functions of  $s$ -wave excitons are shown in Fig. 2. The GPB method is in excellent agreement for the  $1s$  state with the GIBS method, which is performed with no assumptions on the functional form of  $\varphi_{nl}$  and  $F_{nl}$ . This supports the use of the Polmann-Büttner ansatz for extending the calculation to excited states.

Note that the absolute values of exciton eigenenergies,  $|E_{nl}|$ , do not correspond to experimental binding energies,  $E_{nl}^{\text{expt}}$ . In ionic semiconductors free electrons in the conduction band and free holes in the valence band couple to phonons to form polarons. As a result, the measured gap energy  $E_g$  is smaller than the bare gap energy  $E_g^{(0)}$  by an amount equal to the free e-h pair polarization energy,  $\Sigma_0 \equiv \Sigma_e + \Sigma_h$  (see Fig. 1). The experimental binding energies are determined by subtracting the excitonic excitation energies,  $\hbar\omega_{nl}$ , not from the bare gap energy  $E_g^{(0)}$  but from the measured gap energy  $E_g$ . On the other hand, the absolute values of exciton eigenenergies obtained theoretically,  $|E_{nl}|$ , are binding energies from states consisting of a free electron and free hole *not* coupled to phonons, which corresponds to the energies obtained by subtracting  $\hbar\omega_{nl}$  from the bare gap energy  $E_g^{(0)}$ . Therefore, the

TABLE I. Material parameters of CuCl.  $R_{\text{ex}}$  is the phonon radius for the exciton.  $a_0$  and  $a_\infty$  are the Bohr radii estimated with  $\varepsilon_0$  and  $\varepsilon_\infty$ , respectively.  $a_{\text{eff}}$  is the effective exciton radius defined as a radius at the maximum radial probability density. Ryd is the Rydberg energy.

|  | $\varepsilon_0$                      | $\varepsilon_\infty$ | $\mu/m_0$ | $m_e/m_0$ | $m_h/m_0$ | $\hbar\omega_0$ (meV) | $R_{\text{ex}}$ (Å) | $a_0$ (Å) | $a_\infty$ (Å) | $a_{\text{eff}}$ (Å) | Ryd (meV) |
|--|--------------------------------------|----------------------|-----------|-----------|-----------|-----------------------|---------------------|-----------|----------------|----------------------|-----------|
| Extended LLP   |                                      |                      |           |           |           |                       |                     |           |                |                      |           |
| Present  | 6.1                                  | 3.7                  | 0.30      | 0.35      | 1.95      | 25.6                  | 22.4                | 10.9      | 6.6            | 6.9                  |           |
| Ref. [11]  | 7.4                                  | 3.7                  | 0.39      | 0.44      | 3.6       | 27.2                  | 19                  | 10        | 5.0            | 5                    |           |
| Ref. [12]  | 7.4                                  | 3.7                  | 0.39      | 0.44      | 3.6       | 27.2                  | 19                  | 10        | 5.0            |                      |           |
| Refs. [13,14]  | 7.43                                 | 3.73                 | 0.39      | 0.44      | 3.6       | 27.2                  | 19                  | 10.1      | 5.06           | 6.7 <sup>a</sup>     |           |
| Ref. [14]  | 7.43                                 | 3.73                 | 0.35      | 0.392     | 3.17      | 27.2                  | 20                  | 11.2      | 5.64           |                      |           |
| Ref. [17]  | 7.4                                  | 3.7                  | 0.39      | 0.44      | 3.6       | 27.2                  | 20                  | 10        | 5.0            | 10.1                 |           |
| <i>Rydberg series with effective dielectric constant</i> |                                      |                      |           |           |           |                       |                     |           |                |                      |           |
| Ref. [28]  | $\varepsilon_{\text{eff}} \sim 5$    |                      | 0.39      | 0.78      |           |                       |                     |           |                | 7.3                  | 213       |
| Ref. [6]   | $\varepsilon_{\text{eff}} \sim 5.41$ |                      | 0.406     | 0.415     | 20        |                       |                     |           |                | 7.03                 | 189       |
| <i>Mass estimation from experiment</i>                   |                                      |                      |           |           |           |                       |                     |           |                |                      |           |
| Ref. [29]  |                                      |                      | 0.4       | 0.5       | 2.0       |                       |                     |           |                |                      |           |
| Ref. [30]  |                                      |                      | 0.39      | 0.44      | 3.6       |                       |                     |           |                | 7                    |           |
| Ref. [31]  |                                      |                      | 0.39      | 0.43      | 4.2       |                       |                     |           |                | 7                    |           |

<sup>a</sup>The average radius of 10 Å was given in Ref. [13]. The effective exciton radius listed here is estimated by dividing the average radius by 1.5 to compare the effective radius.

energies  $\tilde{E}_{nl} = |E_{nl}| - \Sigma_0$  should be used to compare with the experimental binding energies. In unbounded  $k$ -space,  $\Sigma_0 = \alpha_e \hbar\omega_0 + \alpha_h \hbar\omega_0$ , where  $\alpha_e$  and  $\alpha_h$  are the Fröhlich coupling constants for the electron and the hole, respectively. We calculate  $\Sigma_0 = 123.8$  meV using the parameters in Table I. For application to real solids, however, the sum over  $k$  extends only up to the boundary of the first Brillouin zone. To account for this we use  $\Sigma_0 = \lambda_e \alpha_e \hbar\omega_0 + \lambda_h \alpha_h \hbar\omega_0$ , which is evaluated to be 117.3 meV, where  $\lambda_i = \frac{2}{\pi} \tan^{-1}(k_{\text{max}} R_i)$  and  $k_{\text{max}}$  is the radius of a sphere with the same volume as that of the first Brillouin zone. The effect on the binding energy due to the cutoff in  $k$ -space is significant especially for the 3s and 4s states.

In the present calculation we determined the electron and hole masses of CuCl as  $m_e = 0.35m_0$  and  $m_h = 1.95m_0$ . These masses, however, are quite smaller than those used in earlier calculations,  $m_e \sim 0.4m_0$  and  $m_h \sim 4m_0$ , which were quoted from Ref. [30].

The exciton binding energies  $\tilde{E}_{nl}$  in Table II agree rather well with experimental binding energies. In earlier studies for CuCl [11,12,17] the calculated binding energy of the

TABLE II. Energies of excitons in CuCl.  $E_{nl}$  and  $\tilde{E}_{nl}$  are respectively the eigenenergy and the binding energy calculated by GPB or GIBS.  $E_{nl}^{\text{expt}}$  is the experimental binding energy. The experimental binding energies are estimated using exciton excitation energies [2,21] and the gap energy  $E_g = 3.3990$  eV in Ref. [2]. Energies are in meV.

|                        | GPB                |                   |                   |                  | GIBS               |                   |
|------------------------|--------------------|-------------------|-------------------|------------------|--------------------|-------------------|
|                        | 1s                 | 2s                | 3s                | 4s               | 1s                 | 2p                |
| $-E_{nl}$              | 318.5              | 151.1             | 131.1             | 124.8            | 319.8              | 145.1             |
| $\tilde{E}_{nl}$       | 201.3              | 33.8              | 13.8              | 7.5              | 202.5              | 27.9              |
| $E_{nl}^{\text{expt}}$ | 196.8 <sup>a</sup> | 32.5 <sup>b</sup> | 14.4 <sup>b</sup> | 7.9 <sup>b</sup> | 196.8 <sup>a</sup> | 27.3 <sup>c</sup> |

<sup>a</sup>References [2,21].

<sup>b</sup>Reference [21].

<sup>c</sup>Reference [2].

1s state was quite larger than the experimental energy; for example, the binding energy was reported as  $\tilde{E}_{1s} = 233$  meV in Ref. [17]. Our calculation with updated parameters gives  $\tilde{E}_{1s} = 201.3$  meV.

### III. WAVE FUNCTIONS AND OSCILLATOR STRENGTH

The excitonic orbital functions  $\varphi_{ns}(r)$  multiplied by  $r$  for  $n = 1-4$  are shown in Fig. 2. The Bohr radius defined as  $a_\infty = \varepsilon_\infty \hbar^2 / \mu e^2$  equals 6.6 Å with our CuCl material parameters while  $r\varphi_{1s}(r)$  has a maximum at 6.9 Å. Defining the effective exciton radius  $a_{\text{eff}}$  as a radius of maximum radial probability density of the 1s state, the exciton-phonon interaction increases slightly the effective exciton radius to 6.9 Å.

Compared to the hydrogenic wave functions  $\varphi_{ns}^{\text{H}}(r)$  with  $a_\infty = 6.6$  Å, the excitonic orbital functions are broader in distribution and smaller in amplitude due to the exciton-phonon interaction. The deviations from the hydrogenic wave functions are much more noticeable for states with  $n = 2-4$ , whereas for the 1s exciton the excitonic orbital function is close to the hydrogenic wave function. We can see that the effect of phonon coupling relates to the exciton size compared to the e-h polaron radius  $R_{\text{ex}} = \sqrt{\frac{\hbar}{2\mu\omega_0}}$ , which is 22.4 Å for CuCl. For the 1s state, whose size is much smaller than  $R_{\text{ex}}$ , the electron and the hole in the exciton do not interact strongly with phonons due to screening of the charges, whereas radial states with  $n \geq 2$ , which are larger than  $R_{\text{ex}}$ , are affected considerably by the phonon coupling similar to the strong influence of phonons on the free electron-hole pair.

The oscillator strength of the  $ns$  exciton state is written as

$$f_n \propto |\varphi_{ns}(0)|^2 e^{-g_n(0)}, \quad (17)$$

with

$$g_n(r) = \sum_k |F_{nk}(r)|^2. \quad (18)$$

Figure 3 shows the function  $g_n(r)$  for  $n = 1-4$ . Although  $g_n(r)$ 's are increasing functions for all the states,  $g_1(r)$ , which

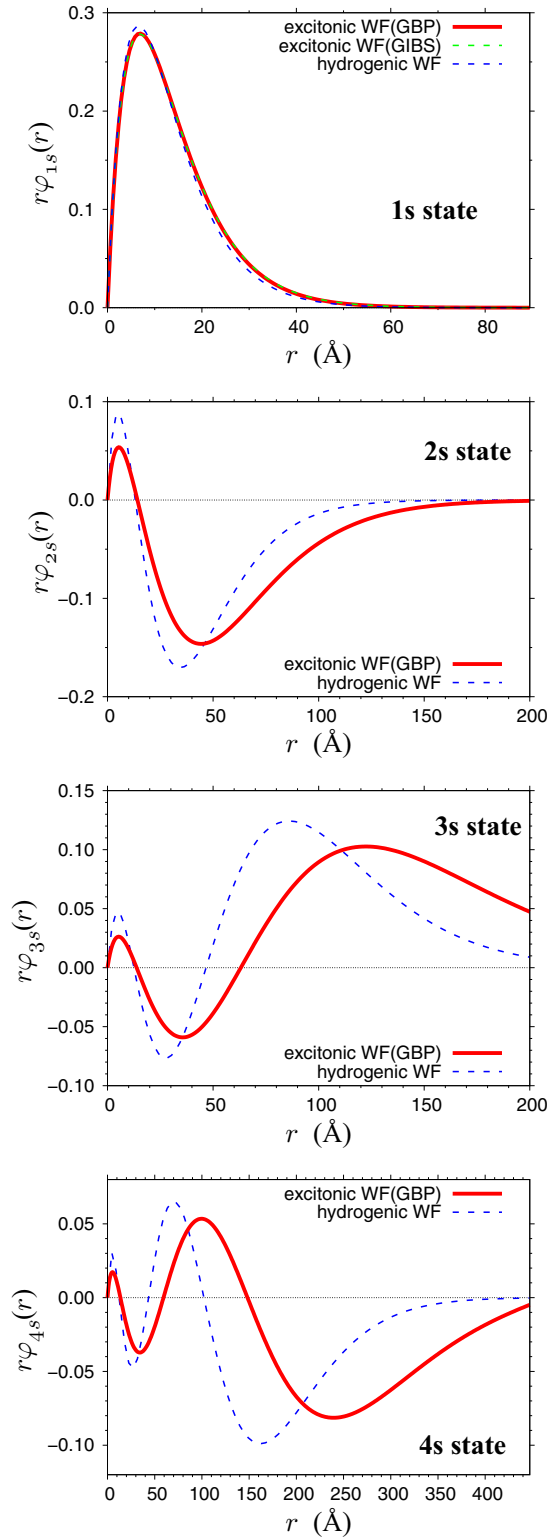


FIG. 2. Excitonic orbital function multiplied by the e-h distance  $r$  for  $n = 1-4$ . The red solid and green dashed curves show excitonic orbital functions obtained using GBP and GIBS methods, respectively. The blue dashed curves are the hydrogenic wave function multiplied by  $r$ .

is for the 1s state, remains relatively small in the whole range of  $r$ . The magnitude of  $g_n(r)$  becomes larger with  $n$  and levels off at  $n \geq 3$ . Thus  $g_n(0)$  causes to suppress

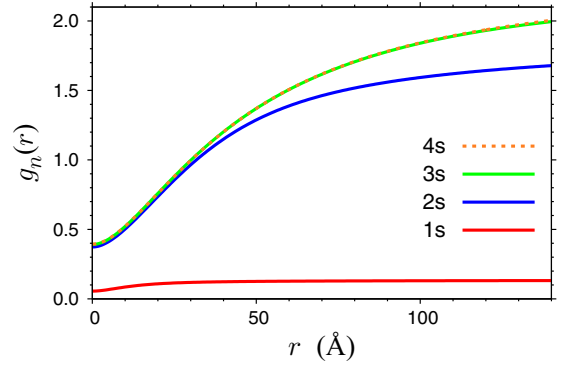


FIG. 3.  $g_n$ 's for  $n = 1-4$  as functions of radius  $r$ .

the oscillator strength especially for  $n \geq 2$ . In addition, the phonon coupling reduces  $\varphi_{ns}(0)$  considerably for  $n \geq 2$  as can be seen from the ratios of  $\varphi_{ns}(0)$  to  $\varphi_n^H(0)$ , which are listed in the second row of Table III. The reduction of  $\varphi_{ns}(0)$  also contributes to reduce the oscillator strengths for  $n \geq 2$ .

Imposing orthogonality of the total wave function as opposed to that of the spatial part alone is essential to correctly determine excited states. For the 2s state the present calculation with the proper orthogonality gives the binding energy as 33.8 meV while a conventional calculation with partial orthogonality gives 33.5 meV. The difference is only about 0.3 meV. However, differences in wave functions are more apparent as shown in Fig. 4. The use of proper orthogonality makes the orbital function smaller at short distances and the function  $g_n$  larger at longer distances.

In the limiting case of vanishing exciton-phonon interaction, i.e.,  $\varphi_{ns}(r) = \varphi_n^H(r)$  and  $g_n(r) = 0$ , the oscillator strength obeys the  $1/n^3$  law:  $f_n/f_1 = 1/n^3$ . In practice, however,  $f_n/f_1$  shifts to a smaller value than  $1/n^3$  since  $f_n$  for  $n \geq 2$  is reduced considerably due to the exciton-phonon interaction, whereas the reduction for  $f_1$  is small. The ratios of  $f_n$  to  $f_1$  are listed in the third row of Table III. We define an oscillator strength reduction factor  $s_n$  as a parameter characterizing the phonon effect on oscillator strength by

$$\frac{f_n}{f_1} = s_n \frac{1}{n^3}. \quad (19)$$

The reduction factors are estimated to be  $s_2 = 0.27$  and  $s_3 = s_4 = 0.22$ . One can see that  $s_n$  converges to approximately 0.22 with increase in  $n$ .

#### IV. DISPERSION ANALYSIS OF INVERSE POLARITON SERIES

The ratios of the oscillator strengths obtained theoretically in the last section can be tested by utilizing measurements

TABLE III. Properties of  $ns$  exciton states with  $n = 1-4$  for CuCl.

| $ns$                          | 1s   | 2s    | 3s     | 4s     |
|-------------------------------|------|-------|--------|--------|
| $\varphi_n(0)/\varphi_n^H(0)$ | 0.95 | 0.58  | 0.53   | 0.53   |
| $f_n/f_1$                     | 1    | 0.034 | 0.0081 | 0.0035 |
| $s_n$                         | 1    | 0.27  | 0.22   | 0.22   |

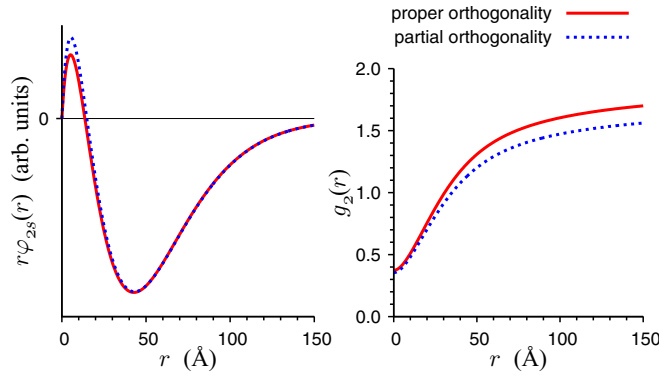


FIG. 4. Comparisons of  $r\varphi_2$  and  $g_2$  using the full orthogonality (red solid line) with those using the partial orthogonality (blue dashed line).

of the inverse polariton series (IPS) in CuCl reported in Refs. [4,21]. The experimental spectral points of the IPS,  $[\mathbf{k}, \omega(\mathbf{k})]$ , are indicated by red dots in Fig. 5. These spectral points correspond to the lower polariton branch (LPB), upper polariton branch (UPB), or higher polariton branches (PB<sub>*ns*</sub> for  $n = 2 - 4$ ). The experimental data can be fitted by the multibranch dispersion of the  $s$ -wave polariton by explicitly accounting for a few lowest energy optically active exciton states as

$$\frac{c^2 k^2}{\omega^2} = \varepsilon_b + \sum_{X(ns)} \frac{\Omega_{X(ns)}^2}{\omega_{X(ns)}^2 - \omega^2}, \quad (20)$$

where  $\hbar\omega_{X(ns)}$  is the excitation energy of the  $X(ns)$  exciton,  $\Omega_{X(ns)}$  is the corresponding Rabi frequency, and  $\varepsilon_b$  is the background permittivity. In the second term of Eq. (20), the summation for  $X(ns)$  is taken over six excitons,  $Z_3(ns)$  with  $n = 1-5$  and the  $1s$  state of  $Z_{12}$  exciton. The exciton energy  $\hbar\omega_{X(ns)}$  has spatial dispersion given by  $\hbar\omega_{X(ns)} = E_{X(ns)} + \frac{\hbar^2 k^2}{2M}$ , where we take  $M = 2.3m_0$  for all the exciton states.

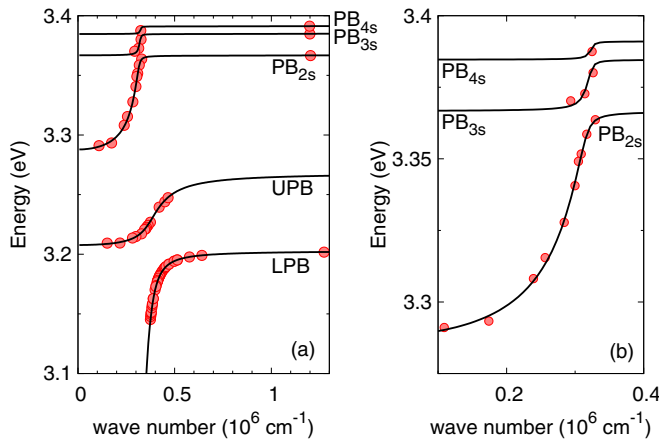


FIG. 5. The multibranch polariton dispersion for CuCl. (b) PB<sub>*ns*</sub> for  $n = 2-4$  in the region where crossing of the dispersion curves is avoided is enlarged. Solid red circles are measured spectral points. The solid curves are theoretical dispersions fitted to the measured spectral points.

TABLE IV. Exciton energies  $E_{X(ns)}$  and Rabi frequencies  $\Omega_{X(ns)}$  for  $Z_3(ns)$  with  $n = 1-4$  and  $Z_{12}(1s)$  for CuCl.

| $X(ns)$      | $E_{X(ns)}$ (eV) | $\hbar\Omega_{X(ns)}$ (meV) |
|--------------|------------------|-----------------------------|
| $Z_3(1s)$    | 3.2022           | 452.4                       |
| $Z_3(2s)$    | 3.3665           | 83.1                        |
| $Z_3(3s)$    | 3.3846           | 40.8                        |
| $Z_3(4s)$    | 3.391            | 26.5                        |
| $Z_{12}(1s)$ | 3.267            | 741.1                       |

Analysis of the dispersion relation for the IPS emissions was also attempted in the previous paper [21]. In that work two assumptions were made with respect to Eq. (20). One was that the exciton wave function was exactly hydrogen-like; thus  $\Omega_{Z_3(ns)}$  followed the  $1/n^3$  law:  $\Omega_{Z_3(ns)}^2/\Omega_{Z_3(1s)}^2 = f_{Z_3(ns)}/f_{Z_3(1s)} = 1/n^3$ . The other was that  $\varepsilon_b$  was a constant. With these assumptions the theoretical dispersion curves approximated well to experimental spectral points for LPB and UPB, whereas the fitting quality was not adequate for PB<sub>*ns*</sub> ( $n \geq 2$ ).

In the present work we modify the assumptions as follows.

*Condition 1.* The  $1/n^3$  law for  $\Omega_{Z_3(ns)}^2$  is violated since the wave function deviates from the hydrogenic form due to the interaction with phonons. Alternatively we have

$$\frac{\Omega_{Z_3(ns)}^2}{\Omega_{Z_3(1s)}^2} = \frac{f_{Z_3(ns)}}{f_{Z_3(1s)}} = \frac{s_n}{n^3}, \quad (21)$$

with  $s_2 = 0.27$  and  $s_3 = s_4 = s_5 = 0.22$ . For  $s_2-s_4$  we used the values in Table III, which are estimated from wave functions. For  $s_5$  we took the same value as  $s_4$  under the presumption of convergence of  $s_n$  in radial states with large  $n$  as mentioned in Sec. II.

*Condition 2.*  $\varepsilon_b$  is approximated by

$$\varepsilon_b(\omega) = \varepsilon_b(0) + \frac{\Omega'^2}{\omega'^2 - \omega^2}, \quad (22)$$

where  $\varepsilon_b(0)$ ,  $\Omega'$ , and  $\omega'$  are adjustable parameters. Here we use a constraint that  $\varepsilon_b(\omega) = 4.3$  for  $\hbar\omega = 3.2$  eV in accordance with Ref. [22].

The background permittivity  $\varepsilon_b$  consists of contributions of oscillators with higher frequency than the gap energy. Hence  $\varepsilon_b$  is in principle written as

$$\varepsilon_b(\omega) = 1 + \sum_i \frac{\Omega_i^2}{\omega_i^2 - \omega^2}. \quad (23)$$

For simplification we replaced Eq. (23) with one representative oscillator represented by Eq. (22).

From analysis of the dispersion relation, the parameters in Eq. (20) are determined as  $\hbar\Omega_{Z_3(1s)} = 452.4$  meV,  $\hbar\Omega_{Z_{12}(1s)} = 741.1$  meV,  $\hbar\Omega' = 3.508$  eV,  $\hbar\omega' = 4.529$  eV, and  $\varepsilon_b(0) = 3.1$ . We list the exciton energies  $E_{X(ns)}$  and the Rabi frequencies  $\Omega_{X(ns)}$  in Table IV. As shown in Fig. 5, the dispersion relation agrees well with experimental spectral points even in the high polariton branches.

The two conditions we imposed are essential to fit the theoretical dispersion of PB<sub>*ns*</sub>'s for  $n \geq 2$  to experiments in the  $k$  region where crossing of dispersion curves is avoided.

TABLE V. Revised material parameters of CuCl.

|                          |                   |
|--------------------------|-------------------|
| Reduced mass             | $0.30m_0$         |
| Electron mass            | $0.35m_0$         |
| Hole mass                | $1.95m_0$         |
| Effective exciton radius | $6.9 \text{ \AA}$ |

$\varepsilon_b(\omega)$  represented by Eq. (20) increases monotonically in the frequency range for exciton excitations. This shifts the avoided-crossing region toward higher wave number than that obtained from the constant  $\varepsilon_b$ . Moreover, gradients of dispersions in this  $k$  range are sensitive to Rabi frequencies. The Rabi frequencies are reduced due to the coupling to phonons compared with those expected from the  $1/n^3$  law, which make the gradients more rapid.

## V. CONCLUSIONS

We used an accurate variational approach for calculating exciton states including polaronic coupling in CuCl. The wave functions of excitons in excited  $s$  states with  $n = 2-4$  are strongly modified by the exciton-phonon interaction. The sizes of the excitons with  $n = 2-4$  are larger than the polaron radius and consequently the corresponding oscillator strengths become much smaller than those predicted by the  $1/n^3$  rule.

The availability of accurate exciton states allows us to analyze the polariton dispersion obtained from inverse polariton series with unprecedented accuracy. We found that the reduction of the oscillator strength due to the phonon effect and the energy dependence of the background permittivity are essential for reproducing the observed dispersion relations in the range  $k = (0.2-0.4) \times 10^6 \text{ cm}^{-1}$ , where crossing of

dispersion curves is avoided. The oscillator strengths obtained from the calculated wave functions are in good agreement with experimental polariton dispersion.

We determined the electron and hole masses of CuCl as  $m_e = 0.35m_0$  and  $m_h = 1.95m_0$  and obtained the effective exciton radius of the  $1s$  state as  $a_{\text{eff}} = 6.9 \text{ \AA}$ . As shown in Table I, these masses are quite smaller than those used in earlier calculations, which were quoted from Ref. [30]. Most of the CuCl effective mass estimations in the 1970s [29–31] were based on exciton energy measurements and the reduced mass ( $\sim 0.39m_0$ ). The reduced mass of about  $0.39m_0$  had been estimated in the 1960s [6,28] by fitting energies of exciton series to a hydrogenic formula with an effective dielectric constant. Although the reduced mass determined by that simple method was not accurate, it has been used for determining the exciton radius as well as the effective masses. Using the reduced mass of  $0.39m_0$  and the effective dielectric constant of about 5, the effective Bohr exciton radius is estimated to be about  $7 \text{ \AA}$ , which was often used for studies on CuCl microcrystals [32–35]. However, the roughly estimated exciton radius was consistent with our effective exciton radius,  $6.9 \text{ \AA}$ . We list the revised material parameters of CuCl in Table V.

Correct interpretation of observed  $1s$ -exciton binding energy as a difference between a much larger Coulomb energy and the polaron energy in the free electron-hole pair shows that the actual Coulomb binding energy of exciton complexes such as the biexciton is much larger than that naively obtained by treating the exciton binding energy as the effective Rydberg. Application of this idea and its importance for accurate modeling of biexcitons is presented in a following paper [8].

## ACKNOWLEDGMENTS

This collaboration work started at JST, ERATO MASUMOTO Single Quantum Dot Project. We would like to thank Prof. Yasuaki Masumoto for his support and many useful discussions during the project.

- 
- [1] H. Haken, *Z. Phys.* **146**, 527 (1956).
  - [2] K. Saito, M. Hasuo, T. Hatano, and N. Nagasawa, *Solid State Commun.* **94**, 33 (1995).
  - [3] H. Matsumoto, K. Saito, M. Hasuo, S. Kono, and N. Nagasawa, *Solid State Commun.* **97**, 125 (1996).
  - [4] E. Tokunaga, A. L. Ivanov, S. V. Nair, and Y. Masumoto, *Phys. Rev. B* **59**, R7837(R) (1999).
  - [5] T. Kazimierzczuk, D. Fröhlich, S. Scheel, H. Stolz, and M. Bayer, *Nature (London)* **514**, 343 (2014).
  - [6] J. Ringeissen and S. Nikitine, *J. Phys. Colloq.* **28**, C3-48 (1967).
  - [7] J. Usukura, Y. Suzuki, and K. Varga, *Phys. Rev. B* **59**, 5652 (1999).
  - [8] J. Usukura, S. V. Nair, and E. Tokunaga, *Phys. Rev. B* **102**, 075203 (2020).
  - [9] R. S. Knox, *Theory of Excitons*, Solid State Physics Suppl. 5 (Academic Press, New York, 1963).
  - [10] J. Pollmann and H. Büttner, *Phys. Rev. B* **16**, 4480 (1977).
  - [11] J. Pollmann and H. Büttner, *Solid State Commun.* **17**, 1171 (1975).
  - [12] E. O. Kane, *Phys. Rev. B* **18**, 6849 (1978).
  - [13] M. Matsuura and H. Büttner, *Phys. Rev. B* **21**, 679 (1980).
  - [14] M. Matsuura and H. Büttner, *Solid State Commun.* **33**, 221 (1980).
  - [15] H. Fröhlich, *Adv. Phys.* **3**, 325 (1954).
  - [16] T. D. Lee, F. E. Low, and D. Pines, *Phys. Rev.* **90**, 297 (1953).
  - [17] G. Iadonisi, F. Bassani, and G. Strinati, *Phys. Status Solidi B* **153**, 611 (1989).
  - [18] T. Mita, K. Sôtome, and M. Ueta, *Solid State Commun.* **33**, 1135 (1980).
  - [19] T. Mita, K. Sôtome, and M. Ueta, *J. Phys. Soc. Jpn.* **48**, 496 (1980).
  - [20] M. Kuwata, T. Kuga, H. Akiyama, T. Hirano, and M. Matsuoka, *Phys. Rev. Lett.* **61**, 1226 (1988).
  - [21] E. Tokunaga, A. L. Ivanov, S. V. Nair, and Y. Masumoto, *Phys. Rev. B* **63**, 233203 (2001).
  - [22] E. Tokunaga, K. Kurihara, M. Baba, Y. Masumoto, and M. Matsuoka, *Phys. Rev. B* **64**, 045209 (2001).
  - [23] B. Hönerlage, A. Bivas, and V. D. Phach, *Phys. Rev. Lett.* **41**, 49 (1978).

- [24] Y. Masumoto, Y. Unuma, Y. Tanaka, and S. Shionoya, *J. Phys. Soc. Jpn.* **47**, 1844 (1979).
- [25] B. Prevot, B. Hennion, and B. Dorner, *J. Phys. C: Solid State Phys.* **10**, 3999 (1977).
- [26] Z. Vardeny and O. Brafman, *Phys. Rev. B* **21**, 2585 (1980).
- [27] K. Wakamura, *Solid State Commun.* **86**, 503 (1993).
- [28] S. Nikitine, in *Progress in Semiconductors*, edited by F. Alan and B. Gibson (Wiley, New York, 1962), Vol. 6, p. 235.
- [29] B. Hönerlage, C. Klingshirn, and J. B. Grun, *Phys. Status Solidi B* **78**, 599 (1976).
- [30] Y. Kato, T. Goto, T. Fujii, and M. Ueta, *J. Phys. Soc. Jpn.* **36**, 169 (1974).
- [31] C. I. Yu, T. Goto, and M. Ueta, *J. Phys. Soc. Jpn.* **34**, 693 (1973).
- [32] A. I. Ekimov, A. L. Efros, and A. A. Onushchenko, *Solid State Commun.* **56**, 921 (1985).
- [33] T. Itoh, Y. Iwabuchi, and M. Kataoka, *Phys. Status Solidi B* **145**, 567 (1988).
- [34] Y. Kayanuma, *Phys. Rev. B* **38**, 9797 (1988).
- [35] Y. Masumoto, S. Okamoto, and S. Katayanagi, *Phys. Rev. B* **50**, 18658 (1994).